Clays and Clay Minerals, Vol. 65, No. 6, 417–430, 2017.

PREPARATION OF ORGANO-MONTMORILLONITES AND THE RELATIONSHIP BETWEEN MICROSTRUCTURE AND SWELLABILITY

Wei Hua Yu[1,2], Ting Ting Zhu[2], Dong Shen Tong[2], Min Wang[2], Qi Qi Wu[2], and Chun Hui Zhou[2,3,4,5]*

[1] Zhijiang College, Zhejiang University of Technology, Shaoxing 312030, China
[2] Research Group for Advanced Materials & Sustainable Catalysis (AMSC), State Key Laboratory Breeding Base of Green Chemistry-Synthesis Technology, College of Chemical Engineering, Zhejiang University of Technology, Hangzhou 310032, China
[3] Centre for Future Materials, University of Southern Queensland, Toowoomba, Queensland 4350, Australia
[4] Engineering Research Center of Non-metallic Minerals of Zhejiang Province, Zhejiang Institute of Geology and Mineral Resource, Hangzhou 310007, China
[5] Qing Yang Institute for Industrial Minerals (QYIM), Youhua Township, Qingyang County, 242804, Anhui, China

Abstract—Hydrophobicity, swellability, and dispersion are important properties for organo-montmorillonites (OMnt) and have yet to be fully characterized for all OMnt configurations. The purpose of the present work was to examine the preparation of OMnt from the reaction of Ca^{2+}–montmorillonite (Ca^{2+}–Mnt) with a high concentration of surfactant and to reveal the relevant properties of hydrophobicity and dispersion of the resultant OMnt. A series of OMnt samples were prepared using a small amount of water and cetyltrimethylammonium bromide (CTAB) with a concentration more than the CTAB critical micelle concentration (CMC). The relationship between OMnt microstructure and the hydrophobicity and swellability properties was investigated in detail. The resulting OMnt samples were characterized using powder X-ray diffraction patterns (XRD), Fourier-transform infrared (FTIR) spectroscopy, thermogravimetric and differential thermogravimetry (TG-DTG), water contact angle tests, swelling indices, and transmission electron microscopy (TEM). The addition of CTAB and water in the OMnt preparation affected the OMnt microstructure and properties. An increase in CTAB concentration led to a more ordered arrangement of cetyltrimethylammonium (CTA^+) cations in the interlayer space of the OMnt and a large amount of CTA^+ cations on the outer surfaces of the OMnt. The swelling indices and the water contact angles of OMnt samples depended on the distribution of the CTAB surfactant on OMnt and the orientation of the surfactant hydrophilic groups on the inner and on the outer surfaces of OMnt. A maximum swelling index of 39 mL/g in xylene was achieved with an average water contact angle of 62.0º ± 2.0º when the amount of CTAB added was 2 times the cation exchange capacity (CEC) of Mnt and the lowest water to dry Mnt mass ratio was 3 during the preparation of OMnt samples. The platelets of OMnt aggregated together in xylene by electrostatic attraction and by hydrophobic interactions.

Key Words—Adsorption, Cetyltrimethylammonium Bromide, CTAB, Hexadecyltrimethylammonium Bromide, Montmorillonite, Organoclay, Surfactant.

INTRODUCTION

Montmorillonite (Mnt), a naturally occurring clay mineral, is an inorganic aluminosilicate with a layered structure (Grim, 1968; Zhu *et al.*, 2015; Hayakawa *et al.*, 2016). Two Si-O tetrahedral sheets surround a central Al-O octahedral sheet to form platelets of Mnt (Zhou *et al.*, 2016a, 2016b; Chen *et al.*, 2017). Some exchangeable cations (*e.g.*, Na^+ and Ca^{2+}) are located in the interlayer space to balance the negative charge of Mnt layers that result from isomorphic substitutions, such as Al^{3+} for Si^{4+} in the tetrahedral sheet and Mg^{2+} for Al^{3+} in the octahedral sheet (He *et al.*, 2005; Szczerba and Kalinichev, 2016). Mnt is hydrophilic with a high swellability in water and a high cationic exchange capacity (Zhou *et al.*, 2012). Mnt can be modified with cationic, anionic, or nonionic surfactants to obtain hydrophobic organo-montmorillonites (OMnts) (Khajehpour *et al.*, 2015; Scholtzov¿ó *et al.*, 2016). OMnts have a broad range of applications as rheological agents, coatings, polymer additives, and adsorbents in wastewater treatment (Bergaya and Lagaly, 2013; Zhou and Keeling, 2013; Yu *et al.*, 2013; Ma *et al.*, 2016; Veiskarami *et al.*, 2016).

The OMnt samples with greater hydrophobic and swelling properties usually disperse well in organic solvents (Hu *et al.*, 2013). The swelling properties depend on the microstructure of OMnt. A number of studies have investigated various ways of preparing OMnt in order to discover the effect of preparation conditions on the OMnt microstructure, which includes Mnt basal spacing expansion, surfactant arrangement in the OMnt interlayer space, and the amount of adsorbed

* E-mail address of corresponding author:
clay@zjut.edu.cn; Chun.Zhou@usq.edu.au
DOI: 10.1346/CCMN.2017.064068

This paper was originally presented during the 3rd Asian Clay Conference, November 2016, in Guangzhou, China.

surfactant (Lin *et al.*, 2011). In OMnt preparation, the amounts of water and surfactant used are key factors. In general, a large amount of water with a high water to Mnt mass ratio of about 100:1−20:1 (*i.e.* 99−95 wt.% water) was used to prepare OMnt samples (Chang *et al.*, 2003; Zhu *et al.*, 2007). The commonly used amount of surfactant is 0.5−2 times the cation exchange capacity (CEC) of Mnt, but in some cases a much larger amount of surfactant (4−11.5 × CEC) was used (Wang and Wang, 2008; Feng *et al.*, 2009; Kooli, 2013). Moslemizadeh *et al.* (2016) reported that the amount of cetyltrimethylammonium bromide (CTAB, equivalent to hexadecyltrimethylammonium bromide) adsorbed onto Mnt and the adsorption isotherms above CTAB critical micelle concentration (CMC) in water were different from those below the CMC by batch equilibrium experiments. The amount of adsorbed CTAB on Mnt increased as the equilibrium CTAB concentrations increased, and the adsorption isotherms fit Langmuir and linear models, which corresponded to monomeric (below the CMC) and micellar (above the CMC) adsorption, respectively. In general, the degree of OMnt surfactant coverage, the basal spacing of OMnt, and the degree of order of surfactant arranged in the OMnt interlayer space increased with an increase in the amounts of surfactant and water used in preparing OMnt. A few studies, however, have reported the synthesis of OMnt prepared using a small amount of water (not more than 75 wt.%) and Mnt in the reaction mixture. Generally, a large amount of water used in the synthesis of OMnt helps Mnt to swell fully and facilitates uniform intercalation of surfactant cations into the Mnt interlayer space (He *et al.*, 2006a). A small amount of water, however, can also lead to large OMnt basal spacings and swelling indices in xylene (Yu *et al.*, 2014). Moreover, the relationships between OMnt microstructure and the above mentioned properties are still unclear.

The present study aimed to explore a more economical and cleaner method to produce OMnt samples with a high swellability and good dispersion in organic solvents. The purpose was to further understand the relationship between OMnt microstructure and the hydrophobic and swellability properties of OMnt samples prepared using small amounts of water (high concentrations of CTAB), using a series of OMnt samples prepared from different initial aqueous CTAB concentrations that ranged from 10.9 up to 138.5 g/L above the CMC of CTAB in water and using 1−2 × CEC of Mnt and 75−95 wt.% water in the preparation mixture (Table 1). A further goal was to determine the effects of water and CTAB on OMnt preparation, microstructure, hydrophobicity, xylene swelling properties, and OMnt platelet assembly and on the mechanisms of CTAB surfactant introduction to Mnt. The synthesis of OMnt using Mnt and such high concentrations of CTAB is novel and of broad interest, particularly in industry.

EXPERIMENTAL

Materials

The natural clay used in the experiments was a Ca-montmorillonite from a bentonite deposit in Heishan, Liaoning, China. The bentonite was used without further purification. The Mnt content of the natural bentonite clay was about 78% as measured using the methylene blue test (Kahr and Madsen, 1995). The Mnt was not separated from the bentonite so, for the purposes of this study, Mnt hereafter refers to the bentonite rather than to a purified fraction from it. The CEC was 57 mmol/100 g as determined using the NH_4^+ exchange and HCHO (formaldehyde) titration method (Zhu *et al*., 2008). The elemental composition was determined using X-ray fluorescence: 71.62% SiO_2, 13.94% Al_2O_3, 2.45% CaO, 3.42% MgO, 1.35% Fe_2O_3, 0.38% Na_2O, 0.41% K_2O, 0.19% TiO_2, and 0.06% P_2O_5. The Mnt was dried at 150°C for 24 h, ground, and passed through a 200 mesh sieve. The Mnt powder was stored in a desiccator until use. The CTAB with a purity of 99.0 wt.% was supplied by Shanghai Bioscience and Technology Co., Ltd., Shanghai, China. Xylene (⩾99.0%) and anhydrous

Table 1. Amounts of CTAB surfactant on OMnt samples and mass loss during thermal treatment.

Sample	CTAB[a] (g/L)	Water[b] (wt.%)	CTAB[c] (mg/g-dry Mnt)	Mass loss[d] (%)				
				Dehydration <184ºC	(1) 184−307ºC	(2) 307−360ºC	(3) 360−500ºC	184−500ºC
OMnt(19)-1CEC	10.9	95	197.3	2.3	3.7	3.9	8.5	16.1
OMnt(6)-1CEC	34.6	86	218.2	2.3	3.9	4.2	9.4	17.5
OMnt(4)-1CEC	51.9	80	221.8	2.5	4.1	4.0	9.6	17.7
OMnt(5)-1.5CEC	62.3	83	303.9	2.6	5.0	5.4	12.3	22.7
OMnt(5)-2CEC	83.0	83	385.9	1.6	13.9	4.3	9.2	27.4
OMnt(3)-2CEC	138.5	75	294.6	2.0	9.8	4.3	8.2	22.3

[a] The CTAB emulsion concentration used in OMnt synthesis.
[b] Water is the mass percent water used in the water and dry Mnt mixture to prepare OMnt samples.
[c] The amount of CTAB loaded onto dry Mnt samples.
[d] Mass loss was obtained from TG data (Figure 3).

https://doi.org/10.1346/CCMN.2017.064068 Published online by Cambridge University Press

ethanol (analytical grade) were purchased from Hangzhou Chemical Reagents Co., Ltd., Hangzhou, China.

Synthesis of OMnt

The OMnt samples were synthesized according to the method described by Yu *et al.* (2014). Weights of CTAB equal to 1 × CEC, 1.5 × CEC, or 2 × CEC of Mnt were dissolved in hot deionized water (45ºC) to obtain aqueous CTAB emulsions. The hot deionized water to dry Mnt mass ratios were 19, 6, 5, 4, or 3. The CTAB emulsion concentrations were 10.9, 34.6, 51.9, 62.3, 83.0, and 138.5 g/L, respectively. Into the above CTAB emulsions, 5 g of dry Mnt were added with strong stirring. For example, 95 g of hot deionized water was used when the hot deionized water to dry Mnt mass ratio was 19 in the aqueous CTAB emulsion. The water to dry Mnt mass ratios were 19, 6, 5, 4, and 3, which corresponded to 95, 86, 83, 80, and 75 wt.% water, respectively, in the reaction mixtures (Table 1). The resultant mixtures were kept at 60ºC for 20 h and then washed with deionized water 3–5 times until the dissolved Br^- ions were removed. The dissolved Br^- ions were detected using $AgNO_3$ solution. The OMnt samples produced were dried at 100ºC for 12 h. The OMnt samples were designated as OMnt(*x*)-*y*CEC, where *x* is the water to dry Mnt mass ratio and *y* is the CTAB amount (*y* = 1 ×, 1.5 ×, and 2 × multiples of Mnt CEC) added to the OMnt preparations.

Characterization

X-ray diffraction (XRD) patterns were measured using a PANalytical X'Pert PRO X-ray diffractometer (PANalytical, Almelo, The Netherlands) operated at 40 kV and 40 mA with Ni-filtered Cu Kα radiation (λ = 0.1542 nm).

Fourier-transform infrared (FTIR) spectra of the samples were collected using a Nicolet 6700 FTIR spectrometer (Thermo-Nicolet, Madison, Wisconsin, USA). The spectra were recorded at a resolution of 4 cm^{-1} in the 400–4000 cm^{-1} range using KBr sample pellets.

The thermogravimetric (TG) and differential thermogravimetric (DTG) curves of the samples were obtained using a Mettler Toledo Star TGA/DSC1 unit (Mettler Toledo Corp., Zurich, Switzerland). The sample was heated at 15ºC/min from room temperature to 800ºC with a N_2 gas flow.

Transmission electron microscopy (TEM) of the OMnt samples was performed using a Tecnai G2 F30 S-Twin transmission electron microscope (Philips-FEI Co., Eindhoven, The Netherlands) with the voltage set at 300 KV. The samples were diluted and dispersed in xylene, dropped onto a C-coated Cu grid, and dried under an infrared heat lamp prior to TEM observation.

The water contact angles of the samples were measured using a Krüss DSA100 (Krüss Company, Hamburg, Germany) contact angle analyzer. The OMnt powder samples were pressed into tablets under a pressure of 15 MPa for 1 min. Single drops of distilled water with a volume of 6 μL were deposited on the surfaces of the OMnt tablets. The measurements were repeated five times for every sample and the average contact angle was calculated. The confidence interval of the contact angles (β) were calculated according to the statistical t-test using equation 1.

$$\text{Contact angle } (\beta) = \bar{\beta} \pm \frac{ts}{\sqrt{n}} \quad (1)$$

where β is the contact angle (in degrees, º), *s* is the standard deviation (in degrees, º), *t* is the confidence factor at a 90% confidence level, and *n* is the number of measurements.

Swelling indices of OMnt were measured in xylene and anhydrous ethanol. When 1 g of the OMnt sample was added into 50 mL of xylene or anhydrous ethanol, the mixture swelled freely at room temperature. After leaving the mixtures static for 90 min, the swelling indices (mL/g) were obtained from the volumes of swollen OMnt samples in the organic media.

RESULTS AND DISCUSSION

XRD patterns

The XRD patterns of the pristine Mnt in comparison to the OMnt samples (Figure 1) indicated d_{001} spacing expansion of the OMnt samples. The pristine Mnt sample exhibited a weak (001) reflection at 5.75º2θ, which corresponds to a d_{001} spacing of 1.54 nm. All the OMnt samples showed (001) reflections between 4.34º and 5.02º2θ with overlapping peaks at 6.04–6.62º2θ. The OMnt samples, therefore, had a typical lamellar structure (Tiwari *et al.*, 2008). Compared to the pristine Ca^{2+}–Mnt, the d_{001} spacing of the OMnt samples increased up to 1.76–2.04 nm because of the large amount of CTA^+ cations intercalated into Mnt interlayers (Zhu *et al.*, 2011). For the OMnt(5)-2CEC and OMnt(3)-2CEC samples, the higher concentrations of CTAB (83.0, 138.5 g/L, and 2 × CEC) used to prepare the samples resulted in the larger d_{001} spacings of 2.04 and 2.00 nm, respectively. The overlapping peaks at 6.04–6.62º2θ corresponded to d_{001} spacings of about 1.34–1.46 nm because a small amount of surfactant (molecules and/or cations) was adsorbed as a monolayer into the interlayer space of Mnt (Zhu *et al.*, 2003; Xi *et al.*, 2005; Yapar *et al.*, 2005). Among the OMnt samples, the OMnt(3)-2CEC sample had the highest relative peak intensity and the smallest half-height peak width for the basal reflection. This observation suggests that the OMnt(3)-2CEC sample had a more ordered structure (Zhuang *et al.*, 2015).

The CTA^+ cations were arranged in the interlayer space of the OMnt samples according to the d_{001} values and the CTAB surfactant molecular configurations (Li

https://doi.org/10.1346/CCMN.2017.064068 Published online by Cambridge University Press

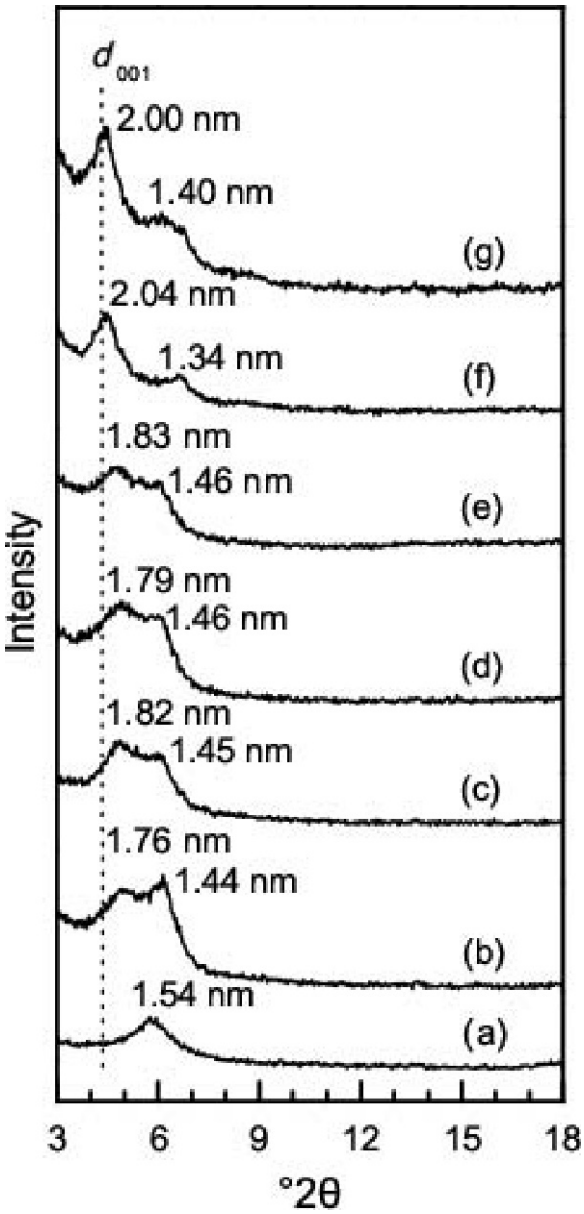

Figure 1. XRD patterns: (a) Ca^{2+}–Mnt; (b) OMnt(19)-1CEC; (c) OMnt(6)-1CEC; (d) OMnt(4)-1CEC; (e) OMnt(5)-1.5CEC; (f) OMnt(5)-2CEC; and (g) OMnt(3)-2CEC.

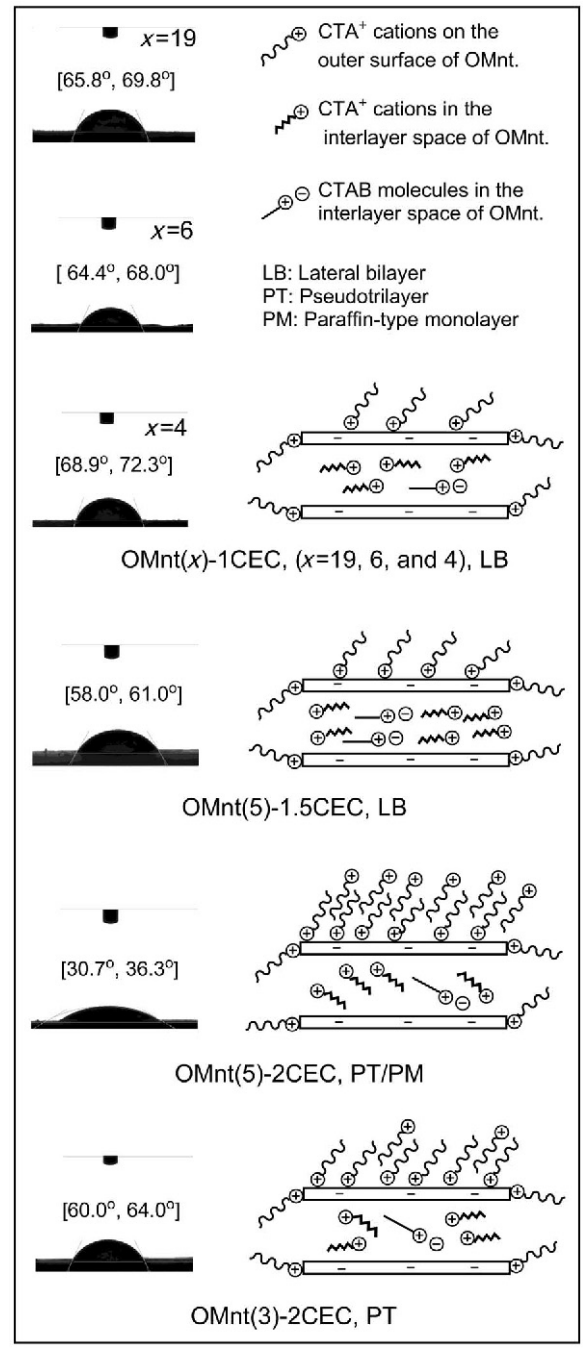

Figure 2. The contact angles of OMnt and models of the arrangement of CTA^+ cations and CTAB molecules.

and Ishida, 2003; Khenifi *et al.*, 2007). The CTA^+ cations adopt a monolayer, a bilayer, a pseudotrilayer, a paraffin-type monolayer, and a paraffin-type bilayer that corresponded to d_{001} values of 1.45–1.47, 1.75–1.85, 1.91–2.02, 2.25–2.50, and 3.85–4.14 nm, respectively, with an increased order in the arrangements (Yu *et al.*, 2014). Thus, for the OMnt(*x*)-1CEC (*x* = 19, 6, and 4) and OMnt(5)-1.5CEC samples, the CTA^+ cations arranged as a bilayer (Zhu *et al.*, 2005; Li *et al.*, 2010). For the OMnt(3)-2CEC sample, the CTA^+ cations adopted a pseudotrilayer arrangement, whereas the CTA^+ cations of the OMnt(5)-2CEC sample took a more ordered all *trans* configuration that was between a pseudotrilayer and a paraffin-type monolayer (Figure 2). The increased CTAB concentrations used in the preparation mixture that ranged from 10.9–62.3 to 138.5 g/L led to a more ordered CTA^+ cation arrangement in the interlayer space of OMnt samples according to the d_{001} values. This result indicates that high CTAB concentrations (83.0, 138.5 g/L, and 2 × CEC) can help

https://doi.org/10.1346/CCMN.2017.064068 Published online by Cambridge University Press

to increase the ordered arrangements of CTA^+ cations in the interlayer space of OMnt samples.

FTIR spectra

The FTIR spectra of the OMnt samples, pure CTAB, and the raw Ca^{2+}–Mnt sample were compared (Figure 3). The pure CTAB surfactant had two pairs of absorbance peaks at 719 and 729 cm^{-1} and at 1464 and 1473 cm^{-1} (Yu *et al*., 2014). The 719 and 729 cm^{-1} absorbance peaks were ascribed to the rocking vibration of $-CH_2$ groups and the 1464 and 1473 cm^{-1} absorbance peaks were ascribed to the scissoring vibration of $-CH_2$ groups (Zhu *et al*., 2005; Xi *et al*., 2007). Furthermore, pure CTAB also showed two absorption bands at 2850 and 2918 cm^{-1}, which correspond to the symmetric and asymmetric stretching vibrations of $-CH_2$ from the CTAB alkyl chains (Li and Ishida, 2003; He *et al*., 2004). For the pristine Ca^{2+}–Mnt sample, none of the strong absorption bands noted above were observed.

After Ca^{2+}–Mnt was modified with CTAB to produce OMnt samples, all the OMnt samples except OMnt(5)-2CEC had broad singlet absorbance peaks at 719 and 1473 cm^{-1}. These singlet absorbance peaks indicate that CTAB molecules or CTA^+ cations adsorbed to OMnt samples had the conformation of a liquid like state (Li *et al*., 2010). The OMnt(5)-2CEC sample exhibited two obvious pairs of absorbance peaks, one pair at 721 and 729 cm^{-1} and another pair at 1464 and 1473 cm^{-1}. The pure solid-state CTAB has similar paired sets of peaks. This result indicates that CTAB molecules or CTA^+ cations adsorbed to OMnt(5)-2CEC had a more ordered solid-like state than those adsorbed to the other OMnt samples (Zhu *et al.*, 2008).

All the OMnt samples exhibited absorption bands at around 2850 and 2918 cm^{-1} similar to pure CTAB, but

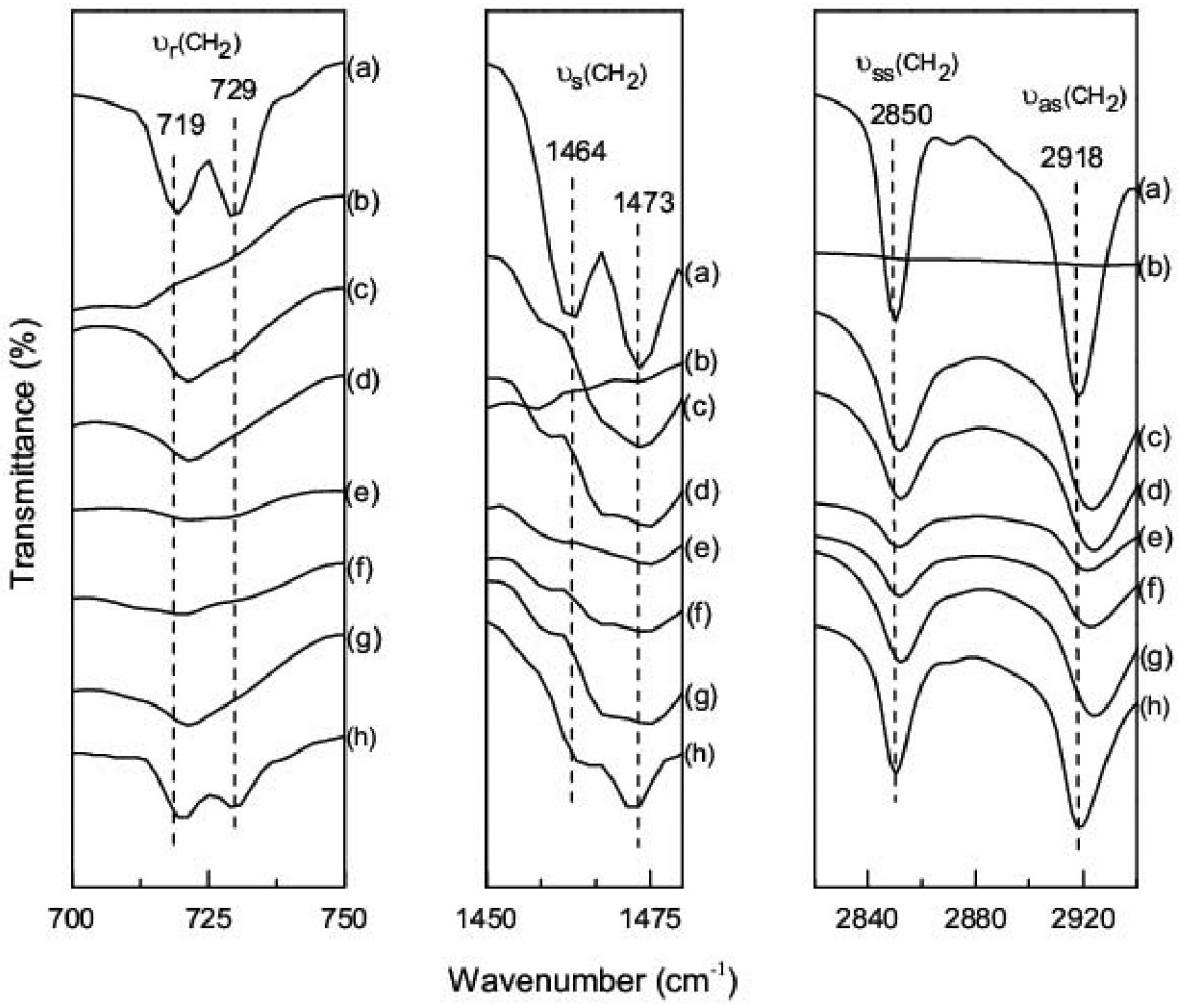

Figure 3. FTIR spectra of (a) pure CTAB; (b) pristine Ca^{2+}–Mnt; (c) OMnt(19)-1CEC; (d) OMnt(6)-1CEC; (e) OMnt(4)-1CEC; (f) OMnt(5)-1.5CEC; (g) OMnt(5)-2CEC; and (h) OMnt(3)-2CEC. $\nu_r(CH_2)$, $\nu_s(CH_2)$, $\nu_{ss}(CH_2)$, and $\nu_{as}(CH_2)$ mean rocking vibration, scissoring vibration, symmetric stretching vibration, and asymmetric stretching vibration of methylene groups in the surfactant.

https://doi.org/10.1346/CCMN.2017.064068 Published online by Cambridge University Press

the pristine Ca^{2+}−Mnt sample did not have these bands. This result indicates that the CTAB surfactant (molecules and cations) were adsorbed to the OMnt samples. For the OMnt(*x*)-1CEC (*x* = 19, 6, and 4) and OMnt(5)-1.5CEC samples, the asymmetric -CH_2 stretching vibrations shifted from 2918 to 2922−2924 cm^{-1}, whereas this band shifted to 2919−2920 cm^{-1} for the OMnt(*x*)-2CEC (*x* = 5 and 3) samples. The absorption band shift from 2918 cm^{-1} to higher wavenumber could be caused by a decrease in the order of the arrangement of CTA^+ cations in the interlayer space of OMnt, such as the change from an ordered solid-state like structure to a disordered liquid-state like structure (Li *et al*., 2010). The observations above indicated that OMnt(5)-2CEC and OMnt(3)-2CEC had more ordered CTA^+ cation arrangements than OMnt(*x*)-1CEC (*x* = 19, 6, and 4) and OMnt(5)-1.5CEC samples because of the greater CTAB concentrations used in the preparation. These results were also confirmed by the XRD data above.

Adsorption mechanisms

The Mnt particles have two kinds of electric charge: A negative structure charge and a variable (pH dependent) charge. The structural negative charge is caused by isomorphous substitution of Mg^{2+}, Fe^{2+}, *etc*. for Al^{3+} in the octahedral sheet and/or Al^{3+} for Si^{4+} in the tetrahedral sheets. Hydroxyl groups are exposed at the broken edges of Mnt platelets. The variable charge results from protonation/deprotonation of these hydroxyl groups and it varies with the pH (van Olphen, 1963; Greaves and Wilson, 1969; Chen *et al.*, 2017). The isoelectric point (pI) of Mnt is 1.47 (de Santana *et al.*, 2006). When the pH is less than the pI, the variable surface charge is positive (Mnt−$AlOH_2^+$), whereas at pHs ⩾ pI, it is negative due to the formation of Mnt−AlO^- groups at the broken edges (Kraepiel *et al.*, 1998; Paget and Simonet, 1994; Yu *et al*., 2013). In the present study, the variable charge of Mnt particles was negative because the pH of the aqueous CTAB emulsion was between 7.1 and 7.3.

The adsorption mechanism of cationic CTAB surfactant onto Mnt involves three possible types of interaction (Scheme 1): (a) Cation exchange to Mnt basal surfaces, (b) hydrophobic interactions of alkyl groups, and (c) electrostatic adsorption to Mnt edges (Dultz *et al*., 2005; Meleshyn and Bunnenberg, 2006). Firstly, when the CTAB surfactant was mixed with Ca^{2+}−Mnt, the hydrated Ca^{2+} in the interlayer space of Mnt was

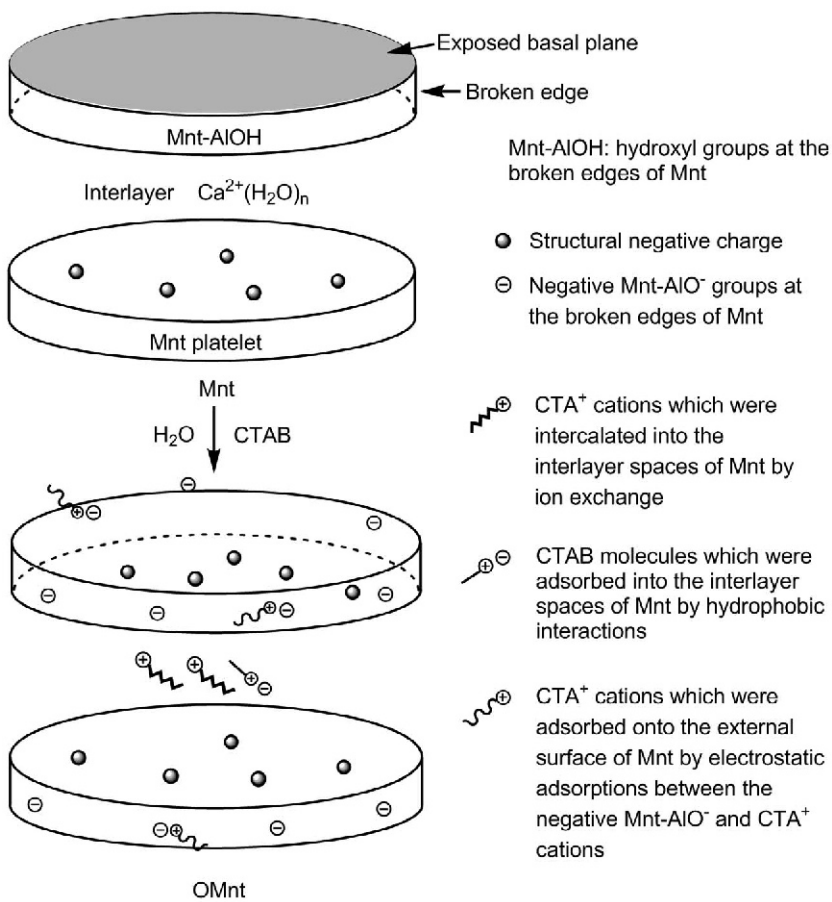

Scheme 1. Adsorption mechanisms of CTA^+ cations and CTAB molecules onto Ca^{2+}−Mnt.

https://doi.org/10.1346/CCMN.2017.064068 Published online by Cambridge University Press

replaced with CTA^+ cations to balance the structural negative charge of Mnt. Secondly, after the CTA^+ cations intercalated into the interlayer space of Mnt, a small number of CTAB molecules (in the form of CTA^+–Br^- ion pairs) were also drawn into the interlayer space of Mnt by hydrophobic bonding because of the long alkyl chains of CTAB (Klebow and Meleshyn, 2012; Chen *et al.*, 2017). Lastly, negative Mnt–AlO^- groups are located at the broken Mnt edges. The CTA^+ cations adsorb onto external surfaces of Mnt by electrostatic interactions between the negative Mnt–AlO^- groups and CTA^+ cations in the CTAB emulsion. These interactions decrease in strength in the order: Ion exchange (electrostatic adsorption within the interlayer space) > electrostatic adsorption (at the edges of clay layers) > hydrophobic interactions of alkyl groups. The strength of the interaction forces affected the thermal stability of CTAB molecules or CTA^+ cations on OMnt and was confirmed by the TG-DTG analysis below. This analysis implied that the CTAB surfactant adsorbed on OMnt had three forms, *i.e.*, (a) CTA^+ cations; (b) CTAB molecules in the interlayer space of OMnt; and (c) CTA^+ cations on the external surfaces of OMnt, respectively. One may assume that no CTAB molecules can exist on OMnt external surfaces because the Br^- ions were removed by washing with water.

TG-DTG analyses

The TG-DTG results (Figure 4) show the thermal stability of CTAB-modified OMnt samples and the amounts of CTAB adsorbed to OMnt. The pure CTAB solid completely decomposed at 194–342ºC. For the pristine Ca^{2+}–Mnt sample, no weight-loss peak was discerned between 184 and 500ºC. This result indicates that the Ca^{2+}–Mnt sample contained little or no organic matter.

Both the OMnt(5)-2CEC and OMnt(3)-2CEC samples had three obvious weight-loss peaks centered at 272, 325, and 439ºC, respectively. At 184–307, 307–360, and 360–500ºC, three stages of surfactant mass losses were observed. Yu *et al.* (2014) reported similar results when CTAB equal to 2 × the CEC of Mnt was used to prepare an OMnt sample. The OMnt(*x*)-1CEC (*x* = 19, 6, and 4) and OMnt(5)-1.5CEC samples had two weight-loss peaks at 325 and 439ºC. Compared to the OMnt(5)-2CEC and OMnt(3)-2CEC samples, the first stage of mass loss at 184–307ºC for OMnt(*x*)-1CEC (*x* = 19, 6, and 4) and OMnt(5)-1.5CEC was less obvious. Based on the analysis of the CTAB adsorption mechanisms above, the three stages of mass loss resulted from the decomposition of (1) CTA^+ cations on the OMnt external surfaces, (2) CTAB molecules, and (3) CTA^+ cations in the interlayer space of OMnt, respectively (Xi *et al.*, 2005).

The difference in the strength of the interactions between Mnt and CTAB surfactant (molecules or cations) led to decomposition at different temperatures

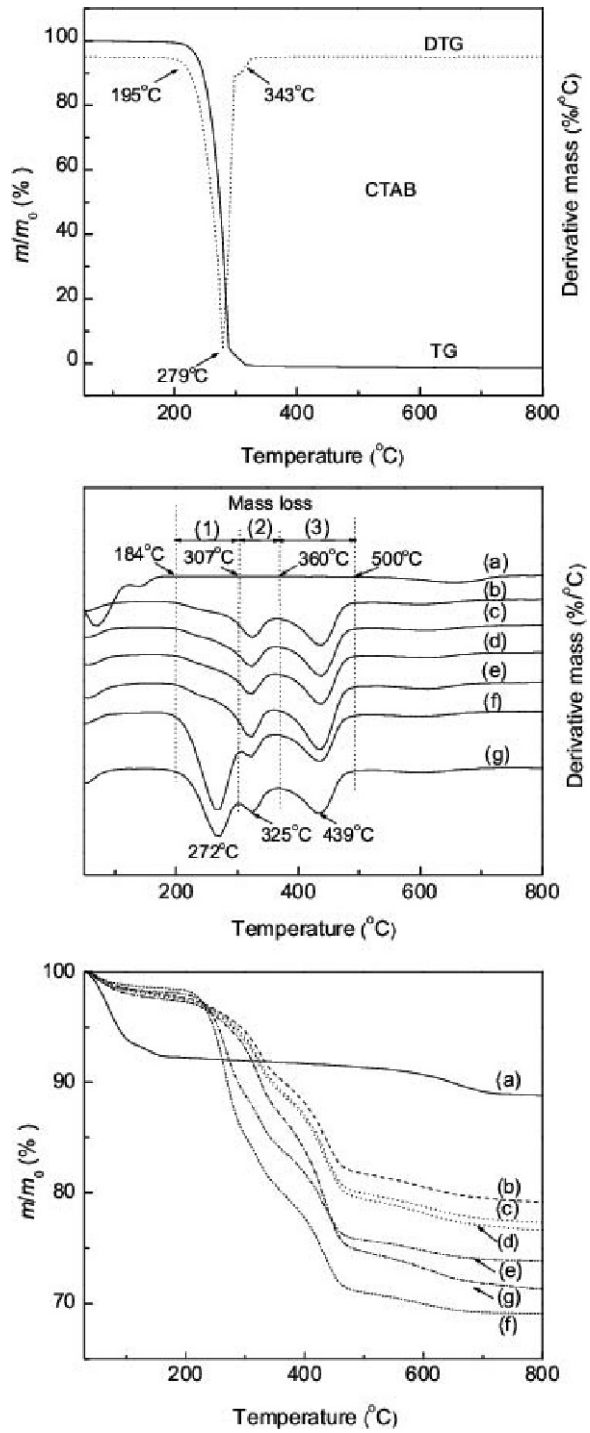

Figure 4. TG-DTG curves of pure CTAB surfactant: (a) Ca^{2+}–Mnt; (b) OMnt(19)-1CEC; (c) OMnt(6)-1CEC; (d) OMnt(4)-1CEC; (e) OMnt(5)-1.5CEC; (f) OMnt(5)-2CEC; and (g) OMnt(3)-2CEC.

(Yu *et al.*, 2014). Ion exchange in the interlayers was the strongest interaction compared with hydrophobic bonding and electrostatic adsorption at the edges of clay layers. Therefore, the CTA^+ cations, which were bound

https://doi.org/10.1346/CCMN.2017.064068 Published online by Cambridge University Press

into the interlayer space of OMnt *via* ion exchange, needed the highest temperatures (360−500ºC) for decomposition and desorption. The surfactant molecules adsorbed by hydrophobic interactions decomposed at 307−360ºC for the different OMnt samples. The higher surfactant decomposition temperatures in the interlayer space were due to protection from the two adjacent Mnt layers. The CTA^+ cations electrostatically adsorbed onto the external surfaces of OMnt were desorbed and decomposed at lower temperatures (184−307ºC) because the surfactant adsorbed at the edges of Mnt layers was more exposed (Xi *et al.*, 2005; He *et al.*, 2006b).

The amounts of CTAB were 17.2, 23.7, and 29.3% (100*CTAB wt./(CTAB wt. + dry Mnt wt.)) and were used to prepare OMnt(*x*)-1CEC (*x* = 19, 6, and 4), OMnt(5)-1.5CEC, and OMnt(*x*)-2CEC (*x* = 3 and 5) samples, respectively. For the OMnt(*x*)-1CEC (*x* = 19, 6, and 4) and OMnt(5)-*y*CEC (*y* = 1.5 and 2) samples, the amounts of CTAB used for OMnt synthesis were near the actual mass losses of total CTAB (16.1−17.7, 22.7, and 27.4%). The actual mass loss of total CTAB for OMnt(3)-2CEC was 22.3%, which is much lower than the amount of CTAB used for OMnt synthesis (29.3%) (Table 1). Moreover, the mass losses of the OMnt(*x*)-2CEC (*x* = 5 and 3) samples were 9.8% and 13.9%, which is higher than the mass losses (3.7−5.0%) of the OMnt(*x*)-1CEC (*x* = 19, 6, and 4) and OMnt(5)-1.5CEC samples at 184−307ºC because the OMnt(*x*)-2CEC (*x* = 5 and 3) samples had more CTA^+ cations adsorbed to external surfaces. The mass losses were similar at both 307−360ºC (3.7−5.4%) and 360−500ºC (8.2−9.6%), except OMnt(5)-1.5CEC had a higher mass loss (12.3%) at 360−500ºC. This result indicates that the high CTAB concentration (2 × CEC) used to prepare the samples facilitated the adsorption of more surfactant onto the OMnt outer surfaces.

The amount of CTAB loaded onto Mnt was found from equation 2.

$$L_{\mathrm{CTAB}} = \frac{1000 \times \mathrm{CTAB}\%}{100\% - \mathrm{H_2O}\% - \mathrm{CTAB}\%} \quad (\mathrm{mgCTAB/g-dryMnt}) \quad (2)$$

where L_{CTAB} is the amount of CTAB (mg/g-dry Mnt) and H_2O% and CTAB% are the mass losses from dehydration and loss of total CTAB, respectively (Table 1).

The amounts of CTAB surfactant adsorbed to dry Mnt increased from 197.3 to 385.9 mg/g-dry Mnt as the CTAB concentration in the CTAB emulsion was increased from 10.9 to 83.0 g/L in the OMnt synthesis (Table 1). This result is consistent with a report that the amount of CTAB adsorbed to Mnt was near 250 mg/g-Mnt when the CTAB equilibrium concentration was about 6 g/L above the CMC (Moslemizadeh *et al.*, 2016). However, the amount of CTAB adsorbed decreased from 385.9 to 294.6 mg/g-dry Mnt with a further increase in the CTAB concentration from 83.0 to 138.5 g/L. This was probably due to the fact that the excess surfactant on OMnt external surfaces was removed when the samples were washed with water.

Distribution of surfactant on OMnt

The distribution of surfactant on OMnt samples (Table 2) was calculated according to published reports (Liu *et al.*, 2011; Xi *et al.*, 2010) using equations 3, 4, and 5:

$$EX_{\mathrm{CTA^+}} = \frac{m_1\% \times 10^5}{284.45 \times (1 - m_1\%) \times \mathrm{CEC}} \quad (3)$$

$$IN_{\mathrm{CTAB}} = \frac{m_2\% \times 10^5}{364.45 \times (1 - m_2\%) \times \mathrm{CEC}} \quad (4)$$

$$IN_{\mathrm{CTA^+}} = \frac{m_3\% \times 10^5}{284.45 \times (1 - m_3\%) \times \mathrm{CEC}} \quad (5)$$

where $EX_{\mathrm{CTA+}}$ is the amount (CEC) of CTA^+ cations absorbed on the outer surfaces of OMnt; IN_{CTAB} and $IN_{\mathrm{CTA+}}$ are the amounts (CEC) of CTAB molecules and CTA^+ cations absorbed in the interlayer spaces of OMnt; m_1%, m_2%, and m_3% are the mass losses (%) of CTAB surfactant at 184−307, 307−360, and 360−500ºC (Table 1); *CEC* is the cation exchange capacity of Mnt (mmol/100g); and 284.45 and 364.45 are the respective molar weights of CTA^+ and CTAB (g/mol).

For all the OMnt samples, the amounts of CTA^+ cations exchanged into the interlayer spaces were about 0.62−0.98 × CEC. Thus, the Ca^{2+} ions in the Mnt interlayer space did not completely exchange with CTA^+ cations. This observation is inconsistent with earlier publications (Feng *et al.*, 2009; Lapides *et al.*, 2011). For the OMnt(5)-1.5CEC sample, a maximum amount of 0.98 × Mnt CEC of CTA^+ cations were exchanged for Ca^{2+} ions. For the OMnt(*x*)-1CEC (*x* = 19, 6, and 4) and OMnt(*x*)-2CEC (*x* = 5 and 3) samples,

Table 2. The distribution of CTAB surfactant on OMnt.

Sample	Amount (CEC)		
	EX_{CTA+} [a]	IN_{CTAB} [b]	IN_{CTA+} [c]
OMnt(19)-1CEC	0.27	0.22	0.62
OMnt(6)-1CEC	0.29	0.25	0.70
OMnt(4)-1CEC	0.31	0.23	0.72
OMnt(5)-1.5CEC	0.40	0.34	0.98
OMnt(5)-2CEC	1.18	0.29	0.78
OMnt(3)-2CEC	0.78	0.27	0.65

[a] EX_{CTA+} is the fraction of the Mnt CEC of CTA^+ cations absorbed on the outer surfaces of OMnt.
[b] IN_{CTAB} and [c] IN_{CTA+}, respectively, are the fractions of CTAB molecules and CTA^+ cations adsorbed in the interlayer space of OMnt.

https://doi.org/10.1346/CCMN.2017.064068 Published online by Cambridge University Press

the amounts of exchanged interlayer CTA^+ cations were similar (0.62−0.78 × CEC). This result indicates that a 62.3 g/L CTAB concentration and a water to Mnt mass ratio of 5 favored more complete cationic exchange in the present work and that CTAB concentrations affect the amount of CTA^+ cations intercalated in OMnt interlayers. Based on the XRD study and the FTIR spectral analysis above, however, the OMnt(5)-1.5CEC sample did not have a more ordered arrangement of interlayer CTAB surfactant cations in comparison to the other OMnt samples.

For all the OMnt samples, approximately 0.22−0.34 × Mnt CEC of the surfactant molecules were adsorbed in the interlayer spaces through hydrophobic interactions and the amounts adsorbed were very similar. This result suggests that the CTAB concentration and the water to Mnt mass ratio had little influence in facilitating CTAB molecule adsorption to the Mnt interlayer spaces by hydrophobic bonding. This finding is similar to our earlier report (Yu *et al*., 2014).

The amounts of CTA^+ cations adsorbed to OMnt external surfaces was between 0.27 and 1.18 × Mnt CEC. For the OMnt(*x*)-1CEC (*x* = 19, 6, and 4) and OMnt(5)-1.5CEC samples, the amounts of CTA^+ cations on external surfaces were similar (0.27−0.40 × Mnt CEC) because the OMnt synthesis was at low CTAB concentrations (10.9−62.3 g/L, 1 × CEC, and 1.5 × Mnt CEC of added CTAB). The high CTAB concentrations (83.0 and 138.5 g/L, 2 × Mnt CEC) helped Mnt to adsorb much more CTA^+ cations (1.18 × and 0.78 × Mnt CEC, respectively) on OMnt external surfaces. Thus, high CTAB concentrations (83.0 and 138.5 g/L, 2 × CEC of CTAB) had a great influence on the amount of CTA^+ cations adsorbed to OMnt(*x*)-2CEC (*x* = 5 and 3) external surfaces.

Based on the observations above, the CTAB emulsion concentration used for OMnt synthesis affected the distribution of adsorbed of CTAB molecules and CTA^+ cations on OMnt external surfaces and interlayers (Xi *et al*., 2005). When the CTAB concentration was <51.9 g/L (1 × Mnt CEC of added CTAB), the adsorbed distributions of CTAB molecules and CTA^+ cations on OMnt were similar. When the CTAB concentration was >62.3 g/L (1.5−2 × Mnt CEC of added CTAB), the distribution of adsorbed CTAB molecules and CTA^+ cations differed significantly.

Contact angles of OMnt

The contact angles between water and OMnt samples can be used to assess the affinity between OMnt and organic media and to quantitatively describe the wettability (Alghunaim *et al*., 2016). The contact angles of water with hydrophilic surfaces is <90º and >90º for hydrophobic surfaces. OMnt samples with larger contact angles have greater surface hydrophobicity. The average contact angle of a hydrophilic Ca^{2+}−Mnt sample was 19.7º, which is close to the reported values for Na^+−Mnt samples (Ballah *et al*., 2016; Zheng and Zaoui, 2017). The average CTAB contact angle was 27.3º. Compared to CTAB and Ca^{2+}−Mnt samples, the contact angles of all the OMnt samples with water were <90º, ranged from 33.5º to 70.6º, and generally increased with CTAB loading (Table 3). The contact angle results indicated that the OMnt surfaces were still hydrophilic (<90º), but more hydrophobic than Ca^{2+}−Mnt surfaces. The average water contact angle values decreased in the order OMnt(4)-1CEC > OMnt(19)-1CEC > OMnt(6)-1CEC > OMnt(3)-2CEC > OMnt(5)-1.5CEC > OMnt(5)-2CEC > Ca^{2+}−Mnt. Four factors affected the water contact angle: (1) The distribution of surfactant on OMnt, (2) the amount of surfactant cations in the OMnt interlayer space, (3) the orientation of surfactant ions on the outer surfaces of OMnt, and (4) the arrangement of the surfactant in the OMnt interlayer space.

The OMnt(*x*)-1CEC (*x* = 19, 6, and 4) samples had comparable average contact angle values of between 66.2º and 70.6º because the surfactant distributions and surfactant arrangements were similar. The OMnt(*x*)-1CEC (*x* = 19, 6, and 4) samples had higher average contact angles than the OMnt(5)-1.5CEC, OMnt(x)-2CEC (*x* = 3 and 5) samples. This result can be explained by the orientations of surfactant ions on the outer surface and in the interlayer space of OMnt. The surfactant hydrophilic groups on the external surface and in the interlayer space

Table 3. The contact angles and swelling indices of OMnt.

Sample	Contact angles (º)	Indices in organic media (mL/g)	
		Xylene	Anhydrous ethanol
Ca^{2+}−Mnt	19.7±2.5	–	–
CTAB	27.3±2.2	–	–
OMnt(19)-1CEC	67.8±2.0	10	6
OMnt(6)-1CEC	66.2±1.8	9	6
OMnt(4)-1CEC	70.6±1.7	11	7
OMnt(5)-1.5CEC	59.5±1.5	26	6
OMnt(5)-2CEC	33.5±2.8	19	5
OMnt(3)-2CEC	62.0±2.0	39	6

± denotes the error determined using the statistical t-test of equation 1.

https://doi.org/10.1346/CCMN.2017.064068 Published online by Cambridge University Press

of the OMnt(x)-1CEC (x = 19, 6, and 4) samples pointed inward, but the hydrophobic surfactant tails were exposed to the outer medium (Figure 2).

The average contact angle of OMnt(5)-1.5CEC was 59.5º, which was close to the 62.0º of OMnt(3)-2CEC. However, the similar hydrophilicity values were caused by different microstructures. The OMnt(5)-1.5CEC sample had the highest amount of exchanged CTA^+ cations ($0.98 \times$ CEC), which caused the hydrophilic groups of some CTA^+ cations in the OMnt inner surface to point outward. In contrast, the orientation of the OMnt(3)-2CEC sample hydrophilic CTA^+ cation groups in the OMnt inner surfaces were similar to those of the OMnt(x)-1CEC (x = 19, 6, and 4) samples because of a low amount of exchanged CTA^+ cations ($0.62-0.72 \times$ CEC). The hydrophilicity of the OMnt (3)-2CEC sample was probably caused by the small amount of the positively charged, excess CTA^+ cation ($0.78 \times$ CEC) head groups on OMnt external surfaces that point outward (Cipriano *et al.*, 2005; Zhuang *et al.*, 2016). Zhuang *et al.* (2015) reported 55º and 50º water contact angles for CTAB-modified OMnt samples, which were prepared using a water to Mnt mass ratio of 30 and amounts of CTAB equal to $1.4\times$ and $2.1 \times$ Mnt CEC. The present work indicates that a small amount of water (water to Mnt mass ratios of 3 and 5) can also be used to prepare CTAB-modified OMnt samples with similar hydrophobicities.

The OMnt(5)-2CEC sample had a minimum average contact angle of 33.5º, which was near the contact angle of pure CTAB (27.3º). The greatest amount of CTA^+ cations ($1.18 \times$ CEC) was on the OMnt(5)-2CEC sample external surfaces and was mainly responsible for the hydrophilicity. A large number of the CTA^+ cation hydrophilic groups (positively charged head) on OMnt sample outer surfaces pointed outward. Moreover, a high amount of exchanged CTA^+ cations ($0.78 \times$ CEC) in the inner surfaces led more of the hydrophilic groups from CTA^+ cations to point outward. This observation is in agreement with the report by Zhuang *et al.* (2015).

Swelling indices of OMnt

The swelling indices of OMnt samples in xylene and anhydrous ethanol (Table 3) indicate that OMnt samples can disperse in solvents with different polarities. According to the swelling index values in liquid media, the materials were divided into zero swelling ($\leqslant$2 mL/g), intermediate swelling (5 $\leqslant$ value $\leqslant$ 8 mL/g), and high swelling (>8 mL/g) (Zhuang *et al.*, 2015). The prepared OMnt samples swelled a lot in xylene, but only to an intermediate extent in anhydrous ethanol. The swelling indices (5−7 mL/g) in anhydrous ethanol in the present work were close to reported values (6.1−9.1 mL/g) for CTAB-modified Mnt (Zhuang *et al.*, 2015). The swelling indices of OMnt were higher in xylene (9−39 mL/g) than in anhydrous ethanol because xylene is less polar than anhydrous ethanol. The solubility of CTAB was greater in anhydrous ethanol than in xylene. Thus, more of the surfactant on the outer surfaces of OMnt was dissolved into anhydrous ethanol than into xylene. The freely dissolved surfactant, therefore, led to decreased swelling indices in anhydrous ethanol (Yu *et al.*, 2014; Moslemizadeh *et al.*, 2016). This observation is consistent with the report that CTAB-modified Mnt had lower swelling indices in nonpolar diesel oil than in polar anhydrous ethanol (Zhuang *et al.*, 2015).

For the OMnt(x)-1CEC (x = 19, 6, and 4) samples, the swelling indices were low (9−11 mL/g) and the values in xylene differed little because of the similar surfactant distributions on the OMnt samples (Table 2). The swelling index of OMnt(3)-2CEC reached a maximum value of 39 mL/g in xylene. These results could be explained by the appropriate amount ($0.78 \times$ Mnt CEC) of surfactant on the outer surfaces and a higher ordering of the OMnt(3)-2CEC structure as discussed above in the *XRD patterns* section and in Zhuang *et al.* (2015). Though the OMnt(5)-2CEC sample had a structural ordering similar to the OMnt(3)-2CEC sample, the OMnt(5)-2CEC sample had a lower swelling index (19 mL/g) in xylene. This result was caused by two probable reasons. On the one hand, the excess surfactant on the outer surface of OMnt(5)-2CEC was easy to desorb. On the other hand, the hydrophilicity of OMnt(5)-2CEC was higher than that of OMnt(3)-2CEC. For the OMnt(5)-1.5CEC sample, the swelling index was 26 mL/g, which is between the swelling index values of the OMnt(3)-2CEC (39 mL/g) and OMnt(5)-2CEC (19 mL/g) samples. This has the same trend as the water contact angle values. Namely, the water contact angle of OMnt(5)-1.5CEC was 59.5 ± 1.5º, which is between the OMnt(3)-2CEC (62.0 ± 2.0º) and OMnt(5)-2CEC (33.5 ± 2.8º) values.

Based on the observation above, the swelling index of OMnt depends on the OMnt surfactant distribution and structural order. The amount ($0.40-1.18 \times$ CEC) of surfactant on the outer surfaces of OMnt and the high contact angle helped to increase the OMnt swelling index and dispersion in xylene. Further, the low water to Mnt mass ratio (*i.e.* 3) used to prepare OMnt(3)-2CEC can also achieve a high swelling index in xylene.

Assembly of clay platelets of OMnt

The microstructures of inorganic Mnt platelets in water after swelling are usually described in terms of edge-to-edge, edge-to-face, and face-to-face (Ebrahimi *et al.*, 2016). Ebrahimi *et al.* (2016) concluded that the face-to-face association was the strongest interaction in clay platelet aggregates in water based on Molecular Dynamics simulations. For Mnt in water and especially for OMnt in an organic medium, however, how the individual clay platelets assemble is still poorly understood. The TEM images of OMnt(3)-2CEC dispersed in xylene (Figure 5) show that the OMnt sample was composed of platelet-like structures and that the OMnt platelets were aggregated

https://doi.org/10.1346/CCMN.2017.064068 Published online by Cambridge University Press

together with sizes of about 10−1000 nm. The results indicated the morphologies of OMnt dispersed in xylene were similar to those of Mnt dispersed in water (Mouzon *et al*., 2016). Pluart *et al*. (2004) also reported that a single platelet of delaminated Mnt had a length of 100−1000 nm, a thickness of 1 nm, and aggregates up to approximately 2−10 μm in water. In the present work, the OMnt clay platelets dispersed in xylene were associated by edge-to-edge (Figure 5b), face-to-face (Figure 5c), and face-to-edge interactions (Figure 5d). The three modes of clay platelet association formed at different OMnt clay platelet sites. The edge-to-edge association was arranged at the broken edges of neighboring clay platelets. The exposed basal planes associated into a face-to-face configuration. The face-to-edge configuration formed between the exposed basal planes and the platelet edges. A detailed description of the interactions between single OMnt platelets is shown in Figure 6. The face-to-face associations depended on the electrostatic interactions between CTA^+ cations and

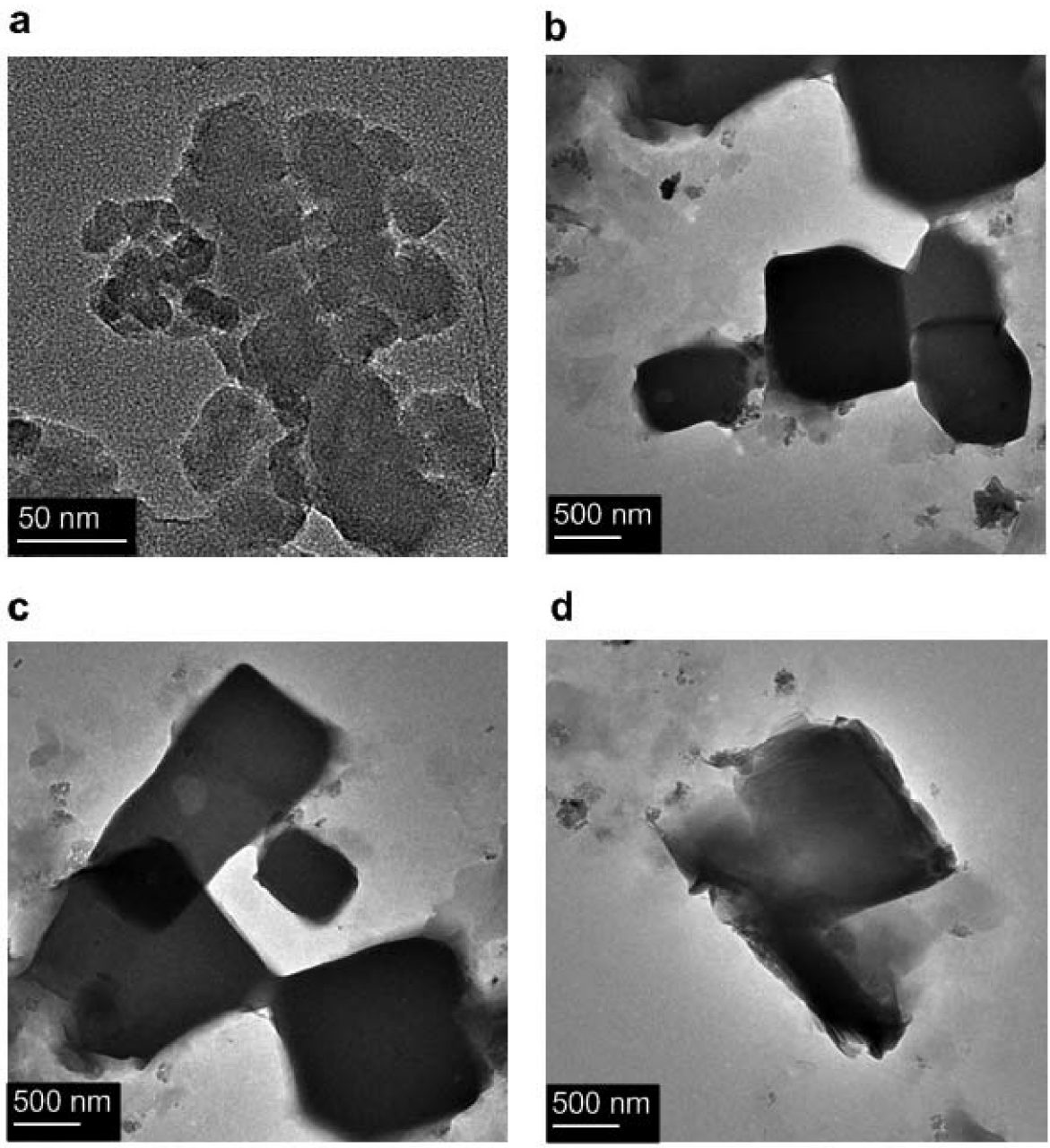

Figure 5. TEM images of OMnt(3)-2CEC: (a) Aggregation of clay platelets in xylene; (b) edge-to-edge association; (c) face-to-face association; and (d) face-to-edge association.

https://doi.org/10.1346/CCMN.2017.064068 Published online by Cambridge University Press

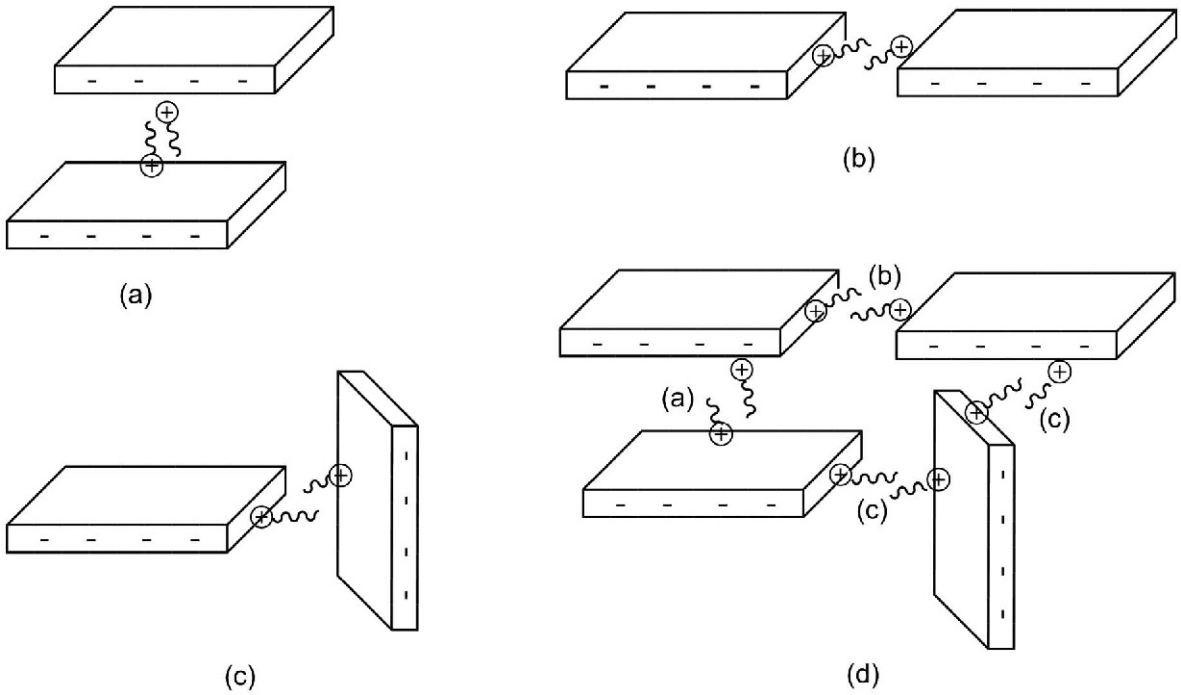

Figure 6. Interactions between platelets of OMnt: (a) Face-to-face interaction; (b) edge-to-edge interaction; (c) face-to-edge interaction; and (d) aggregation by face-to-face, edge-to-edge, and face-to-edge platelets, where ⊕ represents the CTA^+ cations on the edges and the faces of OMnt platelets

negative clay platelets. Both edge-to-edge and edge-to-face associations mainly occurred due to hydrophobic interactions between the CTA^+ cations adsorbed on OMnt broken edge and face surfaces. These observations are in agreement with a report by Burgentzlé *et al.* (2004).

CONCLUSIONS

The present work shows that OMnt can be prepared using high concentrations (10.9 and 138.5 g/L) of aqueous CTAB solutions and Ca^{2+}–Mnt. The Mnt adsorbs the CTAB surfactant by ion exchange in interlayers, hydrophobic interactions, and electrostatic interactions with particle edges. The addition of CTAB and water affected the amount of adsorbed surfactant, the OMnt microstructure, surfactant distribution, hydrophobicity, swellability, and dispersion in xylene. The amount of adsorbed CTAB reached a maximum of 385.9 mg/g-dry Mnt for the OMnt(5)-2CEC sample and a maximum of $1.18 \times$ Mnt CEC of CTA^+ adsorbed to external surfaces. A maximum of $0.98 \times$ Mnt CEC of CTA^+ cations were intercalated into the OMnt(5)-1.5CEC interlayers. The hydrophobicity, swellability, and dispersion of OMnt in xylene depended on the surfactant distribution on OMnt, the orientation of surfactant ions on the OMnt outer surfaces, and the structural arrangement of the surfactant in the OMnt interlayer space. The OMnt(3)-2CEC sample achieved a maximum swelling index (39 mL/g) in xylene. An OMnt sample with a high swelling index can be prepared using a small amount of water. The OMnt clay platelets dispersed in xylene were associated by face-to-face, face-to-edge, and edge-to-edge interactions.

ACKNOWLEDGMENTS

The authors wish to acknowledge the financial support from the National Natural Scientific Foundation of China (41672033; 21373185; 21506188; 21404090); the Distinguished Young Scholar Grants from the Natural Scientific Foundation of Zhejiang Province (ZJNSF, R4100436), ZJNSF (LQ12B03004; LQ14B050001), Zhejiang "151 Talents Project", the projects (2010C14013 and 2009R50020-12) from Science and Technology Department of Zhejiang Provincial Government and the financial support by the open funds from Key Laboratory of Clay Minerals of Ministry of Land and Resources of The People's Republic of China (2014-K02); Engineering Research Center of Non-metallic Minerals of Zhejiang Province (ZD2015k07), Zhejiang Institute of Geology and Mineral Resource, China; and the State Key Laboratory Breeding Base of Green Chemistry-Synthesis Technology, Zhejiang University of Technology (GCTKF2014006), Key Laboratory of High Efficient Processing of Bamboo of Zhejiang Province (2016), and State Key Laboratory of Chemical Resource Engineering, Beijing University of Chemical Technology, China (CRE-2016-C-303).

REFERENCES

Alghunaim, A., Kirdponpattara, S., and Newby, B.M.Z. (2016) Techniques for determining contact angle and wettability of powders. *Powder Technology*, **287**, 201–215.

https://doi.org/10.1346/CCMN.2017.064068 Published online by Cambridge University Press

Ballah, J., Chamerois, M., Durand-Vidal, S., Malikova, N., Levitz, P., and Michot, L.J. (2016) Effect of chemical and geometrical parameters influencing the wettability of smectite clay films. *Colloids and Surfaces A: Physicochemical and Engineering Aspects*, **511**, 255-263.

Burgentzlé, D., Duchet, J., Gérard, J.F., Jupin, A., and Fillon, B. (2004) Solvent-based nanocomposite coatings: I. Dispersion of organophilic montmorillonite in organic solvents. *Journal of Colloid and Interface Science*, **278**, 26−39.

Chang, J.H., An, Y.U., Cho, D., and Giannelis, E.P. (2003) Poly(lactic acid) nanocomposites: Comparison of their properties with montmorillonite and synthetic mica (II). *Polymer*, **44**, 3715−3720.

Chen, H.F., Koopal, L.K., Xiong, J., Avena, M., and Tan, W.F. (2017) Mechanisms of soil humic acid adsorption onto montmorillonite and kaolinite. *Journal of Colloid and Interface Science*, **504**, 457−467.

Cipriano, B.H., Raghavan, S.R., and McGuiggan, P.M. (2005) Surface tension and contact angle measurements of a hexadecyl imidazolium surfactant adsorbed on a clay surface. *Colloids and Surfaces A: Physicochemical and Engineering Aspects*, **262**, 8−13.

De Santana, H., Toni, L.R.M., Benetoli, L.O.B., Zaia, C.T.B.V., Zaia, D.A.M., and Rosa, M. (2006) Effect in glyphosate adsorption on clays and soils heated and characterization by FT-IR spectroscopy. *Geoderma*, **136**, 738−750.

Dultz, S., Riebe, B., and Bunnenberg, C. (2005) Temperature effects on iodine adsorption on organo-clay minerals: II. Structural effects. *Applied Clay Science*, **28**, 17−30.

Ebrahimi, D., Pellenq, R.J.M., and Whittle A.J. (2016) Mesoscale simulation of clay aggregate formation and mechanical properties. *Granular Matter*, **18**, 49.

Feng, X., Hua, G., Meng, X., Ding, Y., Zhang, S., and Yang, M. (2009) Influence of ethanol addition on the modification of montmorillonite by hexadecyl trimethylammonium bromide. *Applied Clay Science*, **45**, 239−243.

Greaves, M. P. and Wilson, M. J. (1969) The adsorption of nucleic acids by montmorillonite. *Soil Biology and Biochemistry*, **1**, 317−323.

Grim, R.E. (1968), *Clay Mineralogy*, 2nd edition. McGraw Hill, New York.

Hayakawa, T., Minase, M., Fujita, K.I., and Ogawa, M. (2016) Modified method for bentonite purification and characterization; A case study using bentonite from Tsunagi Mine, Niigata, Japan. *Clays and Clay Minerals*, **64**, 275-282.

He, H.P., Frost, R.L., and Zhu, J.X. (2004) Infrared study of $HDTMA^+$ intercalated montmorillonite. *Spectrochimica Acta Part A: Molecular and Biomolecular Spectroscopy*, **60**, 2853−2859.

He, H.P., Ding, Z., Zhu, J.X., Yuan, P., Xi, Y.F., Yang, D., and Frost, R.L. (2005) Thermal characterization of surfactant-modified montmorillonites. *Clays and Clay Minerals*, **53**, 287−293.

He, H.P., Frost, R.L., Bostrom, T., Yuan, P., Duong, L., Yang, D., Xi, Y.F., and Kloprogge, J.T. (2006a) Changes in the morphology of organoclays with $HDTMA^+$ surfactant loading. *Applied Clay Science*, **31**, 262−271.

He, H.P., Zhou, Q., Martens, W.N., Kloprogge, J.T., Yuan, P., Xi, Y.F., Zhu, J.X., and Frost, R.L. (2006b) Microstructure of $HDTMA^+$−modified montmorillonite and its influence on sorption characteristics. *Clays and Clay Minerals*, **54**, 691−698.

Hu, Z., He, G., Liu, Y., Dong, C., Wu, X., and Zhao, W. (2013) Effects of surfactant concentration on alkyl chain arrangements in dry and swollen organic montmorillonite. *Applied Clay Science*, **75−76**, 134−140.

Kahr, G. and Madsen, F.T. (1995) Determination of the cation exchange capacity and the surface area of bentonite, illite and kaolinite by methylene blue adsorption. *Applied Clay Science*, **9**, 327−336.

Khenifi, A., Bouberka, Z., Sekrane, F., Kameche, M., and Derriche, Z. (2007) Adsorption study of an industrial dye by an organic clay. *Adsorption-Journal of the International Adsorption Society*, **13**, 149−158.

Khajehpour, M., Gelves, G.A., and Sundararaj, U. (2015) Modification of montmorillonite with alkyl silanes and fluorosurfactant for clay/fluoroelastomer (FKM) nanocomposites. *Clay and Clay Minerals*, **63**, 1−14.

Klebow, B. and Meleshyn, A. (2012) Monte Carlo study of the adsorption and aggregation of alkyltrimethylammonium chloride on the montmorillonite−water interface. *Langmuir*, **28**, 13274−13283.

Kooli, F. (2013) Effect of C16TMA contents on the thermal stability of organo-bentonites: *In situ* X-ray diffraction analysis. *Thermochimica Acta*, **551**, 7−13.

Kraepiel, A.M.L., Keller, K., and Morel, F.M.M. (1998) On the acid−base chemistry of permanently charged minerals. *Environmental Science & Technology*, **32**, 2829−2838.

Lagaly, G., Ogawa, M., and Dékány, I. (2013) Clay mineral-organic interaction. Pp. 435−505 in: *Handbook of Clay Science: Part A, Fundamentals*. Developments in Clay Science. (F. Bergaya and G. Lagaly, editors), Elsevier, Amsterdam.

Lapides, I., Borisover, M., and Yariv, S. (2011) Thermal analysis of hexadecyltrimethylammonium-montmorillonites. *Journal of Thermal Analysis and Calorimetry*, **105**, 921−929.

Li, Y. Q. and Ishida, H. (2003) Concentration-dependent conformation of alkyl tail in the nanoconfined space: Hexadecylamine in the silicate galleries. *Langmuir*, **19**, 2479−2484.

Li, Z.H., Jiang, W.T., Chen, C.J., and Hong, H.L. (2010) Influence of chain lengths and loading levels on interlayer configurations of intercalated alkylammonium and their transitions in rectorite. *Langmuir*, **26**, 8289−8294.

Lin, K.J., Jeng, U.S., and Lin, K.F. (2011) Adsorption and intercalation processes of ionic surfactants on montmorillonite associated with their ionic charge. *Materials Chemistry and Physics*, **131**, 120−126.

Liu, B., Wang, X., Yang, B., and Sun, R. (2011) Rapid modification of montmorillonite with novel cationic Gemini surfactants and its adsorption for methyl orange. *Materials Chemistry and Physics*, **130**, 1220−1226.

Ma L., Zhu, J., Xi, Y., Zhu, R., He, H., Liang, X., and Ayoko, G.A. (2016) Adsorption of phenol, phosphate and Cd(II) by inorganic-organic montmorillonites: A comparative study of single and multiple solute. *Colloids and Surfaces A−Physicochemical and Engineering Aspects*, **497**, 63−71.

Meleshyn, A. and Bunnenberg, C. (2006) Interlayer expansion and mechanisms of anion sorption of Na-montmorillonite modified by cetylpyridinium chloride: A Monte Carlo study. *The Journal of Physical Chemistry B*, **110**, 2271−2277.

Moslemizadeh, A., Aghdam, S.K., Shahbazi, K., Aghdam, H.K., and Alboghobeish, F. (2016) Assessment of swelling inhibitive effect of CTAB adsorption on montmorillonite in aqueous phase. *Applied Clay Science*, **127−128**, 111−122.

Mouzon, J., Bhuiyan, I.U., and Hedlund, J. (2016) The structure of montmorillonite gels revealed by sequential cryo-XHR-SEM imaging. *Journal of Colloid and Interface Science*, **465**, 58−66.

Paget, E. and Simonet, P. (1994). On the track of natural transformation in soil. *FEMS Microbiology Ecology*, **15**, 109-117.

Pluart, L., Duchet, J., Sautereau, H., Halley, P., and Gerard, J.F. (2004) Rheological properties of organoclay suspen-

sions in epoxy network precursors. *Applied Clay Science*, **25**, 207– 219.

Scholtzová, E., Madejová, J., Jankovič, L.U., and Tunega, D. (2016) Structural and spectroscopic characterization of montmorillonite intercalated with N-butylammonium cations (N = 1–4) – Modeling and experimental study. *Clays and Clay Minerals*, **64**, 401–412.

Szczerba, M. and Kalinichev, A.G. (2016) Intercalation of ethylene glycol in smectites: Several molecular simulation models verified by X-ray diffraction data. *Clays and Clay Minerals*, **64**, 488–502.

Tiwari, R.R., Khilar, K.C., and Natarajan, U. (2008) Synthesis and characterization of novel organo-montmorillonites. *Applied Clay Science*, **38**, 203–208.

van Olphen, H. (1963) *Introduction to Clay Colloid Chemistry*. Interscience Publishers, New York.

Veiskarami, M., Sarvi, M.N., and Mokhtari, A.R. (2016) Influence of the purity of montmorillonite on its surface modification with an alkyl-ammonium salt. *Applied Clay Science*, **120**, 111–120.

Wang, L. and Wang, A. (2008) Adsorption properties of Congo red from aqueous solution onto surfactant-modified montmorillonite. *Journal of Hazardous Materials*, **160**, 173–180.

Xi, Y.F., Frost, R.L., He, H.P., Kloprogge, J.T., and Bostrom, T. (2005) Modification of Wyoming montmorillonite surfaces using a cationic surfactant. *Langmuir*, **21**, 8675–8680.

Xi, Y.F., Zhou, Q., Frost, R.L., and He, H.P. (2007) Thermal stability of octadecyltrimethylammonium bromide modified montmorillonite organoclay. *Journal of Colloid and Interface Science*, **311**, 347–353.

Xi, Y.F., Mallavarapu, M., and Naidu, R. (2010) Preparation, characterization of surfactants modified clay minerals and nitrate adsorption. *Applied Clay Science*, **48**, 92–96.

Yapar, S., Özbudak, V., Dias, A., and Lopes, A. (2005) Effect of adsorbent concentration to the adsorption of phenol on hexadecyltrimethyl ammonium-bentonite. *Journal of Hazardous Materials*, **121**, 135–139.

Yu, W. H., Li, N., Tong, D.S., Zhou, C.H., Lin, C.X., and Xu, C.Y. (2013) Adsorption of proteins and nucleic acids on clay minerals and their interactions: A review. *Applied Clay Science*, **80–81**, 443–452.

Yu, W.H., Ren, Q.Q., Tong, D.S., Zhou, C.H., and Wang, H. (2014) Clean production of CTAB-montmorillonite: Formation mechanism and swelling behavior in xylene. *Applied Clay Science*, **97–98**, 222–234.

Zheng, Y. and Zaoui, A. (2017) Wetting and nanodroplet contact angle of the clay 2:1 surface: The case of Na-montmorillonite (001). *Applied Surface Science*, **396**, 717–722.

Zhou, C.H. and Keeling, J. (2013) Fundamental and applied research on clay minerals: From climate and environment to nanotechnology. *Applied Clay Science*, **74**, 3–9.

Zhou, C.H., Zhang, D., Tong, D.S., Wu, L.M., Yu, W.H., and Ismadji, S. (2012) Paper-like composites of cellulose acetate-montmorillonite for removal of hazardous anionic dye in water. *Chemical Engineering Journal*, **209**, 223–234.

Zhou, C.H., Zhao, L.Z., Wang, A.Q., Chen, T.H., and He, H.P. (2016a) Current fundamental and applied research into clay minerals in China. *Applied Clay Science*, **119**, 3–7.

Zhou, D., Zhang, Z., Tang, J., Wang, F., and Liao, L. (2016b) Applied properties of oil-based drilling fluids with montmorillonites modified by cationic and anionic surfactants. *Applied Clay Science*, **1–8**, 121–122.

Zhuang, G., Zhang, Z., Fu, M., Ye, X., and Liao, L. (2015) Comparative study on the use of cationic–nonionic-organo-montmorillonite in oil-based drilling fluids. *Applied Clay Science*, **116–117**, 257–262.

Zhuang, G., Zhang, Z., Sun, J., and Liao, L. (2016) The structure and rheology of organo-montmorillonite in oil-based system aged under different temperatures. *Applied Clay Science*, **124**, 21–30.

Zhu, L.Z., Zhu, R.L., Xu, L.H., and Ruan, X.X. (2007) Influence of clay charge densities and surfactant loading amount on the microstructure of CTMA–montmorillonite hybrids. *Colloids and Surfaces A: Physicochemical and Engineering Aspects*, **304**, 41–48.

Zhu, J.X., He, H.P., Guo, J.G., Yang, D., and Xie, X.D. (2003) Arrangement models of alkylammonium cations in the interlayer of $HDTMA^+$ pillared montmorillonites. *Chinese Science Bulletin*, **48**, 368–372.

Zhu, J.X., He, H.P., Zhu, L.Z., Wen, X.Y., and Deng, F. (2005) Characterization of organic phases in the interlayer of montmorillonite using FTIR and ^{13}C NMR. *Journal of Colloid and Interface Science*, **286**, 239–244.

Zhu, J.X., Wang, T., Zhu, R.L., Ge, F., Yuan, P., and He, H.P. (2011) Expansion characteristics of organo montmorillonites during the intercalation, aging, drying and rehydration processes: Effect of surfactant/CEC ratio. *Colloids and Surfaces A: Physicochemical and Engineering Aspects*, **384**, 401–407.

Zhu, R.L., Zhu, L.H., Zhu, J.X., and Xu, L.H. (2008) Structure of cetyltrimethylammonium intercalated hydrobiotite. *Applied Clay Science*, **42**, 224–231.

Zhu, R., Zhou, Q., Zhu, J., Xi, Y., and He, H. (2015) Organoclays as sorbents of hydrophobic organic contaminants: sorptive characteristics and approaches to enhancing sorption capacity. *Clays and Clay Minerals*, **63**, 199-221.

(*Received 13 April 2017; revised 25 September 2017; Ms. 1174; AE: H. He*)